Nitrogen-Doped Carbonized Polymer Dots: A Potent Scavenger and Detector Targeting Alzheimer's β-Amyloid Plaques

Weiqun Gao, Wenjuan Wang, Xiaoyan Dong, and Yan Sun*

The fibrillization and deposition of β-amyloid protein (Aβ) are recognized to be the pathological hallmarks of Alzheimer's disease (AD), which signify the need for the effective detection and inhibition of Aβ accumulation. Development of multifunctional agents that can inhibit Aβ aggregation, rapidly disaggregate fibrils, and image aggregates is one of the effective strategies to treat and diagnose AD. Herein, the multifunctionality of nitrogen-doped carbonized polymer dots (CPDs) targeting Aβ aggregation is reported. CPDs inhibit the fibrillization of Aβ monomers and rapidly disintegrate Aβ fibrils by electrostatic interactions, hydrogen-bonding and hydrophobic interactions with Aβ in a time scale of seconds to minutes. Moreover, the interactions make CPDs label Aβ fibrils and emit enhanced red fluorescence by the binding, so CPDs can be used for in vivo imaging of the amyloids in transgenic *Caenorhabditis elegans* CL2006 as an AD model. Importantly, CPDs are demonstrated to scavenge the in vivo amyloid plaques and to promote the lifespan extension of CL2006 strain by alleviating the Aβ-triggered toxicity. Taken together, the multifunctional CPDs show an exciting prospect for further investigations in Aβ-targeted AD treatment and diagnosis, and this study provides new insight into the development of carbon materials in AD theranostics.

1. Introduction

Alzheimer's disease (AD), as the most common form of dementia, is an irreversible and chronic neurodegenerative disease.[1–5] Pathologically, the fibrillization and accumulation of amyloid β-protein (Aβ) in patients' brains are the main hallmark of AD. Aβ is formed as a cleavage product of amyloid precursor protein by β- and γ-secretases, and $A\beta_{40}$ is the most abundant form in human cerebrospinal fluid (CSF).[6] The fibrillogenesis of Aβ from soluble monomers to toxic Aβ oligomers and fibrils is thought to be directly related to the neuronal synaptic dysfunction, neuron death, and ultimately collapse of the nervous system.[7,8] Therefore, the development of anti-amyloid agents to modulate Aβ aggregation is proposed to be pivotal for AD prevention and treatment.

Many inhibitors against amyloidosis have been reported, including small molecules,[9–11] peptides,[12,13] proteins,[14,15] and nanomaterials.[16–21] Their properties in electrostatic, hydrogen bonding (H-bonding), π–π stacking, and hydrophobic interactions with Aβ are utilized to disrupt the process of Aβ aggregation and alleviate Aβ toxicity. Of various nanoparticles, graphene quantum dots (GQDs) have been recently employed for detecting Aβ monomers;[22] improving learning and memory capabilities;[23] inhibiting Aβ, α-synuclein, or human islet amyloid polypeptide aggregation;[24–26] and triggering disaggregation of α-synuclein fibrils.[27] Yang et al. synthesized nitrogen-doped carbonized polymer dots (CPDs) as fluorescent probes for biological imaging in vitro and in vivo.[28,29] CPDs as a kind of carbon dots show many excellent characteristics, such as long-wavelength excitation and emission, good biocompatibility, desired blood brain barrier penetration ability, and high quantum yield.[30] Moreover, the red fluorescence of CPDs has less phototoxicity to tissues, lower biological fluorescence background, and higher tissue penetration ability than other short-wavelength fluorescence probes.[29,31–33]

Herein, we report the newly discovered functions of CPDs in inhibiting Aβ fibrillogenesis, rapidly disaggregating Aβ mature fibrils, and emitting enhanced red fluorescence once binding to Aβ aggregates. We have systematically investigated the effects of CPDs on $A\beta_{40}$ monomers/fibrils by an array of in vitro biophysical and biochemical methods and in vivo assays with an AD model of *C. elegans* CL2006 were conducted to investigate the multifunctionality of CPDs.

W. Gao, W. Wang, Prof. X. Dong, Prof. Y. Sun
Department of Biochemical Engineering
School of Chemical Engineering and Technology
Tianjin University
Tianjin 300350, China
E-mail: ysun@tju.edu.cn
Prof. X. Dong, Prof. Y. Sun
Key Laboratory of Systems Bioengineering and Frontiers Science Center
for Synthetic Biology (Ministry of Education)
Tianjin University
Tianjin 300350, China

ADVANCED
SCIENCE NEWS
www.advancedsciencenews.com

NANO · MICRO
small
www.small-journal.com

2. Results and Discussion

2.1. Synthesis and Characterization of CPDs

As shown in **Scheme 1**, CPDs were synthesized by the one-pot hydrothermal method with minor modification.[28] The size distribution of CPDs was relatively uniform, with an average size of 5.0 ± 1.6 nm and well dispersed in the TEM imaging (**Figure 1**a). Well-resolved lattice fringes with spacings of 0.22, 0.26, and 0.32 nm were observed from the high-resolution TEM images of CPDs (Figure 1b), which are close to the (100), (020), and (002) diffraction facets of graphene carbon.[28,34] From the fast Fourier transform of Figure 1-b2 shown in Figure 1-b4, electron diffraction points of the hexagonal honeycomb structure can be seen, indicating that CPDs had a hexagonal crystal structure.[35]

The elemental composition and structure of CPDs were analyzed by X-ray photoelectron spectrometry (XPS). The full XPS energy spectrum of CPDs in Figure 1c shows three peaks at 284.2, 399.1, and 532.1 eV, which are attributed to carbon (C, 75.8%), nitrogen (N, 10.0%), and oxygen (O, 14.2%), respectively. The high-resolution C 1s spectrum of CPDs indicates the existence of $C = C/C−C$ (284.3 eV), $C−N$ (284.9 eV), $C−O$ (285.9 eV), and $C = N$ (286.9 eV), and the high-resolution N 1s spectrum displays four peaks at 398.9, 399.9, 401.7, and 406.6 eV, which respectively represent pyridinic N, pyrrolic N, graphitic N, and $−NO_2$ bonds (Figure 1d). The functional groups on the surfaces/borders of CPDs were determined by Fourier transform infrared (FTIR) spectroscopy. As shown in Figure 1e, the double peaks at 3356 and 3425 $cm^{−1}$ represent the free $−NH_2$ on the surfaces/borders of CPDs, and the peak at 3100 $cm^{−1}$ is attributed to the stretching vibration of $= C−H$ on the surface of benzene rings. The peaks at 1583 and 1619 $cm^{−1}$ are due to the stretching vibrational absorptions of $C = N$ and the $C = C$ double bond in the benzene rings. The peaks at 1224 and 1382 $cm^{−1}$ represent the stretching vibration absorptions of $C−O$ and $−NO_2$. Finally, the characteristic peaks of bending vibration of C-H out-of-plane in the aromatic benzene rings with phenazine skeleton are presented at 604 and 747 $cm^{−1}$.[28,36] It is demonstrated that the benzene rings of CPDs contain heteroatom oxygen and the residual nitro group in the electrophilic reaction of nitric acid with *o*-phenylenediamine under the hydr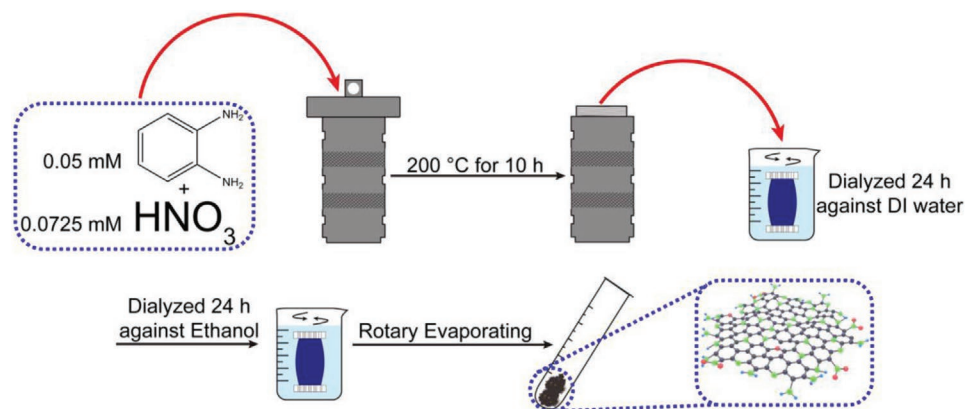othermal reaction. Therefore, the above results suggest that the backbone of CPDs is at least composed of $−NH_2$, $−NO_2$, pyrimidine rings, pyrrole rings, and benzene rings.

From the 3D excitation-emission matrix fluorescence spectrum of CPDs (Figure 1f), two peaks located at the excitation/emission wavelengths (Ex/Em) of nearly 560/627 and 610/627 nm were observed. CPDs showed a maximum emission at 627 nm when excited at 610 nm, and the emission spectrum was independent of the excitation wavelength (Figure 1f), consistent with the previous report.[28] The chromaticity coordinates of CPDs (0.676, 0.310) were calculated according to the fluorescence emission spectrum of CPDs under 610 nm excitation, and are shown in the chromaticity diagram (Figure S1, Supporting Information), confirming the red fluorescence of CPDs excited at 610 nm excitation.

In the CPDs formed by cross-linking and carbonization, the electron-withdrawing groups (-NO_2) produced by the electrophilic reaction of nitric acid with *o*-phenylenediamine under hydrothermal conditions and the electron-donating groups (-NH_2) retained by *o*-phenylenediamine are connected to the conjugated system composed of pyrimidine rings, pyrrole rings, and benzene rings. Because of the presence of these groups, the electron cloud fluidity of the conjugated system will increase, the energy level difference of $π–π^*$ transition will decrease, and the nonradiative transitions in CPDs will be limited, accordingly forcing excited electrons back to the ground state through radiative transitions. Therefore, CPDs can show red fluorescence by covalent-bond crosslink-enhanced emission (CEE).[37] The red emission signals were observed by fluorescence microscopy excited at 535/50 nm with a long-pass emission filter at 590 nm (Figure S2b,d, Supporting Information), and the fluorescence intensity of CPDs is higher in 3.0% ethanol solution than in aqueous solution due to the increased solubility. Therefore, 3.0% ethanol was used as solvent in the following experiments to ensure good dispersion of CPDs. Here, it should be noted that in vivo dispersion of CPDs can also be facilitated by protein corona and other factors.[38]

2.2. Inhibition on A$β_{40}$ Aggregation

The fluorescence dye thioflavin T (ThT) that shows enhanced fluorescence when binding to amyloid fibrils rich in $β$-sheet structures is commonly used to detect amyloid fibrils.[39,40]

Scheme 1. Schematic representation of the synthesis of CPDs from *o*-phenylenediamine and nitric acid.
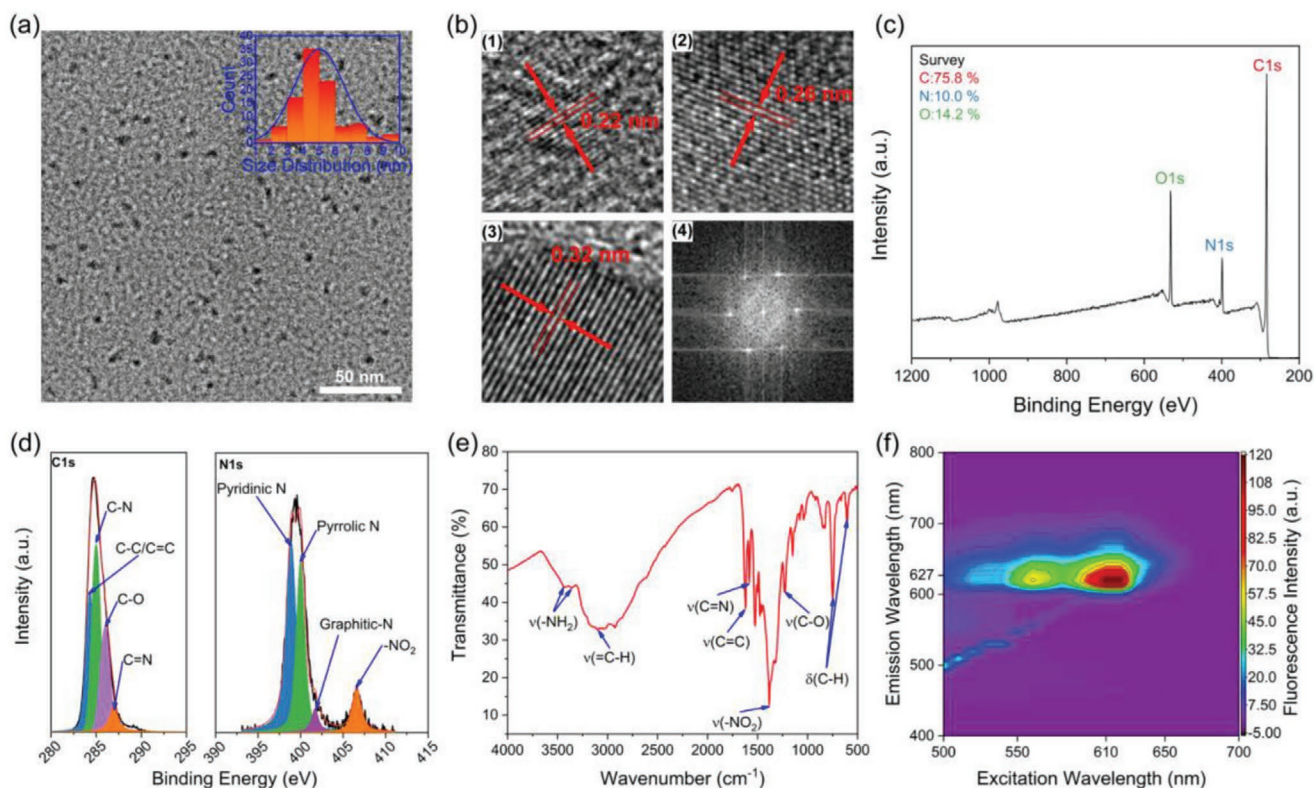
Figure 1. Characterization of CPDs. a) TEM image. The inset shows the size distribution. b) High-resolution TEM images show well-resolved lattice fringes (b1–b3); (b4) is the fast Fourier transform image of (b2). c) XPS energy spectrum. d) High-resolution C1s XPS (left), and N1s XPS spectrum (right). e) FTIR spectrum. f) 3D excitation-emission matrix fluorescence spectrum (3D EEMS).

Because CPDs had no interference on ThT fluorescence intensity at different concentrations (Figure S3, Supporting Information), in situ ThT fluorescence assay was conducted with $A\beta_{40}$ to investigate the effect of CPDs on $A\beta$ fibrillization. As depicted in **Figure 2**a, the kinetics of $A\beta_{40}$ aggregation alone showed a sigmoidal curve with an obvious lag phase that corresponds to the nucleation period. CPDs effectively prevented $A\beta_{40}$ fibrillization in a dose-dependent manner, as evidenced by the decreased ThT fluorescence intensity of the plateau phase and the elongation rates with the increase of CPDs concentrations (Figure S4 and Table S1, Supporting Information). CPDs at 100 µg mL^{-1} significantly inhibited the $A\beta_{40}$ ThT fluorescence intensity by 74.1% and reduced the elongation rate of $A\beta_{40}$ to 0.15 ± 0.02 h^{-1}, which was only 16.0% that of $A\beta$ alone $(0.94 \pm 0.06$ h$^{-1})$, as shown in Figure S4 and Table S1, Supporting Information. Moreover, CPDs shortened the lag time (T_{lag}) of $A\beta_{40}$ with increasing dose (Figure 2b), indicating that CPDs could increase the nucleation of $A\beta_{40}$. As shown in Figure 1d,e, the CPDs are abundant in -NH$_2$ and exhibit a positive ζ-potential (+3.6 mV) in HEPES buffer (pH = 7.4), while $A\beta_{40}$ presents a negative net charge.[41] Therefore, CPDs could interact with $A\beta_{40}$ via electrostatic attractions, H-bonding, and hydrophobic interactions, leading to a high local concentration of $A\beta_{40}$ monomers on the surfaces/borders. An elevated concentration at surfaces/borders would increase the nucleation or shorten the lag time, as indicated in literature.[42,43] However, the CPDs could effectively suppress $A\beta_{40}$ fibril elongation (Figure 2a and Figure S4, Supporting Information). These are the sequential

effects of CPDs in two different stages. Therefore, it may be possible to improve the inhibition capabilities of CPDs by charge regulation.

The secondary structural change of $A\beta$ from random coil to β-sheet is a characteristic phenomenon of $A\beta$ fibrillization. Therefore, far-UV circular dichroism (CD) spectroscopy was used to gain an insight into the effects of CPDs on $A\beta_{40}$ conformational transition. The initial secondary structure of $A\beta_{40}$ without (Figure 2c, dash line) or with CPDs (Figure S5, Supporting Information) presented a random coil conformation with a negative peak at 197 nm.[15,44] After 72 h incubation, one positive peak at 196 nm and one negative valley at 215 nm appeared for the $A\beta_{40}$ only group, indicating the formation of β-sheet structures.[45,46] With increasing CPDs concentration, the negative ellipticity value at 215 nm progressively decreased, implying the decrease of β-sheet content of $A\beta_{40}$ aggregates. These results demonstrate that CPDs could effectively inhibit the transformation of $A\beta_{40}$ to β-sheet-rich aggregates.

The morphology of $A\beta_{40}$ aggregates incubated without or with CPDs was visualized by atomic force microscopy (AFM) (Figure 2d). $A\beta_{40}$ alone formed long and dense fibrillar networks, similar to previous reports.[46,47] By contrast, after incubation with CPDs, the content of $A\beta_{40}$ fibrils decreased significantly, and $A\beta_{40}$ fibrils became short, dispersed, and broken. These phenomena became particularly significant when the CPDs concentration was as high as 100 µg mL^{-1}. Moreover, dot-blot assays with OC (anti-amyloid fibrils) further confirmed the potency of CPDs on inhibiting $A\beta_{40}$ fibrillization. As shown
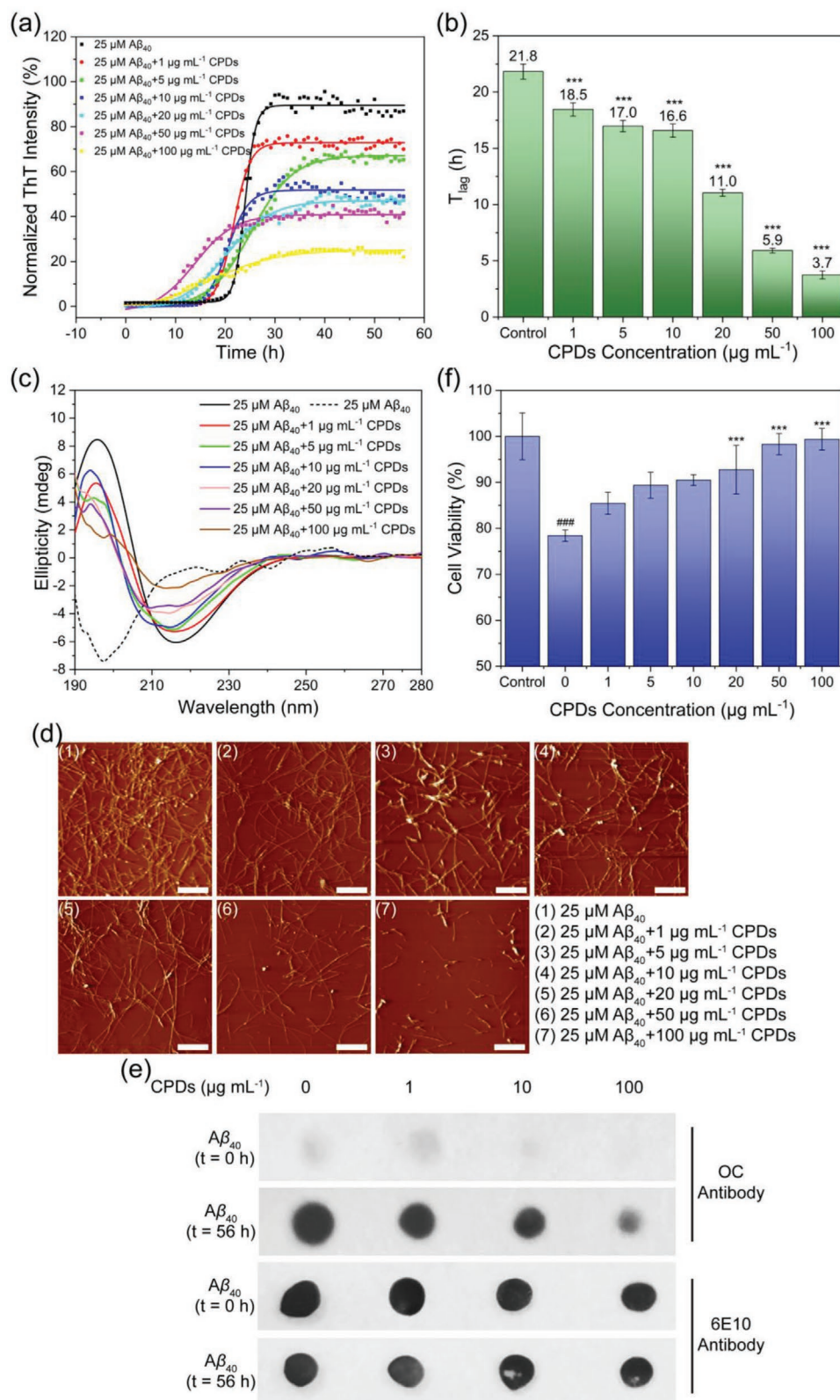
Figure 2. Inhibition of $A\beta_{40}$ aggregation by CPDs by 56 h co-incubation at 37 °C. a) The kinetics of $A\beta_{40}$ aggregation in the absence or presence of CPDs. b) Lag time values of $A\beta_{40}$ aggregation with CPDs. *** ($p < 0.001$) compared to the $A\beta_{40}$-only group (Control group). Data in (a) and (b) were obtained by triplicate experiments, and error bars in graph represent the mean ± SD ($n = 3$). c) Far-UV circular dichroism spectra of $A\beta_{40}$ aggregates with CPDs. d) AFM images of $A\beta_{40}$ incubated with or without CPDs. Scale bar, 2 µm. e) Dot-blot assay showing $A\beta_{40}$ fibrils levels at the initial and final

in Figure 2e, few Aβ_{40} fibrils were formed in the presence or absence of CPDs at the beginning (0 h), and the amount of OC reactive fibrils formed at 56 h significantly decreased with increasing CPDs concentration. The same membranes were also immunostained with 6E10 (anti-Aβ_{1-16}) antibody to confirm identical loadings of Aβ_{40} species.

3-(4,5-Dimethyl-2-thiazolyl)-2,5-diphenyltetrazolium bromide (MTT) assays were performed with SH-SY5Y cells to evaluate the biocompatibility and detoxification of CPDs on the amyloid. As displayed in Figure S6, Supporting Information, 3.0% ethanol and 1–100 µg mL^{-1} CPDs exhibited no significant toxicity to SH-SY5Y cells. Similar observation that low-concentration ethanol (<0.64 g kg^{-1}) was almost non-toxic for mice was reported.[48,49] This demonstrates the safety of the presence of 3.0% ethanol in the sample for in vivo experiments. The cell viability decreased to 78.4% after treating SH-SY5Y cells with the pre-incubated Aβ_{40} species for 24 h (Figure 2f). CPDs alleviated the toxicity of Aβ_{40} in a dose-dependent manner, which is consistent with the above ThT, CD, and AFM results. Remarkably, 100 µg mL^{-1} CPDs rescued cell viability to 99.4%, proving that CPDs were a potent modulator against the cytotoxicity of Aβ_{40} aggregates.

From the results discussed above, we can conclude that CPDs could suppress Aβ_{40} fibrillization by preventing the conformational transition of Aβ to β-sheet-rich structures, leading to the reduction of fibrils formation and the low-toxicity. The inhibitory effect of CPDs is comparable to that of other nanomaterials reported previously, such as casein coated-gold nanoparticles (βCas AuNPs), GQDs, graphene quantum dot-tramiprosate (GQD-T), and carbon-dots (C-Dots).[24,50–52] However, those materials were not reported to show any capabilities of disaggregating mature Aβ fibrils, which is what to be discussed next for the present CPDs.

2.3. Disaggregation of Aβ_{40} Fibrils

The disruption or remodeling of existing Aβ fibrils is an important therapeutic strategy for AD treatment,[53,54] so the ability of CPDs to disaggregate mature Aβ_{40} fibrils was evaluated. CPDs led to a dramatic decrease of ThT fluorescence intensity within 4 h in a dose-dependent manner, as shown in **Figure 3**a, implying the disassembly of Aβ_{40} fibrils by CPDs. Moreover, the incubation of mature Aβ_{40} fibrils with CPDs showed a reduction in CD signals of the β-sheet structure as compared to those of Aβ_{40} fibrils alone (Figure 3b). The CD signal intensity of Aβ_{40} at 215 nm gradually changed from −6.28 to −1.70 mdeg by adding 0 to 100 µg mL^{-1} CPDs, implying that CPDs effectively remodeled Aβ_{40} mature fibrils into aggregates with lower β-sheet structures. CPDs have unique chemical compositions such as amino, nitro, pyrimidine rings, pyrrole rings, and benzene rings, so there could be multiple interactions, such as electrostatic interactions, H-bonding, and hydrophobic interactions, between CPDs and Aβ fibrils, which might lead

to the breaking of intermolecular Aβ salt bridges and disruption of highly ordered fibrillar structures stabilized by these interactions.[43,55,56]

The ThT results (Figure 3a) indicate that the disassembly of Aβ fibrils was quite fast, finishing in less than 4 h. Therefore, to see more details in the disassembly, fast disaggregation kinetics of Aβ_{40} fibrils modulated with CPDs was investigated by stopped-flow fluorescence spectroscopy (Figure 3c). From the fast kinetic curves, the ThT fluorescence intensity of Aβ_{40} fibrils treated with CPDs exhibited a rapid decrease within 50 s, then continued to decline slowly, indicating that CPDs disrupted Aβ_{40} fibrils on a time scale of seconds. Then, the fast disaggregation of Aβ_{40} mature fibrils by CPDs was investigated by AFM observations at different CPDs concentrations and time intervals (Figure 3d and Figure S7, Supporting Information). Although CPDs at low concentrations (<10 µg mL^{-1}) showed relatively weak remodeling effects, fibrils became less and shorter over time, while Aβ_{40} fibrils without CPDs treatment kept a long and dense fibrillar morphology (Figure S7, Supporting Information). Notably, effective degradation of Aβ_{40} fibrils was observed by CPDs at 100 µg mL^{-1}; significant fibrils reduction occurred by only 5–10 min incubation, and only a few completely crushed aggregates remained after depolymerization for 4 h (Figure 3d). In dot-blot assays, Aβ_{40} fibrils (25 µM) was incubated with CPDs (1, 10, and 100 µg mL^{-1}). The amount of OC reactive fibrils was maximum at 0 h, which confirms the abundant of Aβ fibrils species at the beginning (Figure 3e). The intensity of OC reactive fibrils significantly decreased with increasing CPDs concentration after 4 h disassembly, which is in agreement with the AFM imaging results (Figure 3d and Figure S7, Supporting Information). Similar with the tests of aggregates described above, the same membranes immunostained with 6E10 (anti-Aβ_{1-16}) antibody confirmed identical loadings of Aβ_{40} species (Figure 3e). Because disruption of Aβ fibrils might lead to the formation of toxic Aβ oligomers,[13,57,58] Aβ_{40} oligomers in the disaggregation process were detected by A11 antibody and illustrated in Figure S8, Supporting Information. As compared to that treated without CPDs (Figure S8a, Supporting Information), no detectable dot-blot spot of the products of Aβ_{40} fibrils treated with CPDs (Figure S8b, Supporting Information) indicates that the disaggregation of Aβ_{40} fibrils by CPDs did not result in the formation of soluble oligomers. Above results denote that the CPDs could rapidly disrupt Aβ_{40} mature fibrils into non-oligomeric species in the first 50 s, and remodel the conformation of Aβ_{40} aggregates from high β-sheet structures in 4 h.

It should be noted that, to the best of our knowledge, this rapid disaggregation of Aβ has not been reported in literature with any other agents, either small molecules or carbon-based nanomaterials. For example, epigallocatechin gallate (EGCG), brazilin, and tanshinones could remodel large amyloid fibrils into small, off-pathway unstructured forms by over 24 h or even 48 h.[10,59–62] Moreover, previous studies demonstrated that graphitic carbon nitride (g-C$_3$N$_4$)

time points of inhibition. Aβ_{40} (25 µM) was incubated with CPDs (1, 10, and 100 µg mL^{-1}) in HEPES buffer (20 mM HEPES, 100 mM NaCl, pH = 7.4) at 37 °C under 150 rpm. The samples were spotted onto nitrocellulose membrane, and probed with anti-amyloid fibrils OC antibody and anti-Aβ_{1-16} 6E10 antibody. f) The inhibitory effect of CPDs on Aβ_{40} induced cytotoxicity toward SH-SY5Y. ### ($p < 0.001$), as compared to the control group. *** ($p < 0.001$), as compared to the Aβ_{40}-treated group. Error bars in graph represent the mean ± SD ($n = 6$).
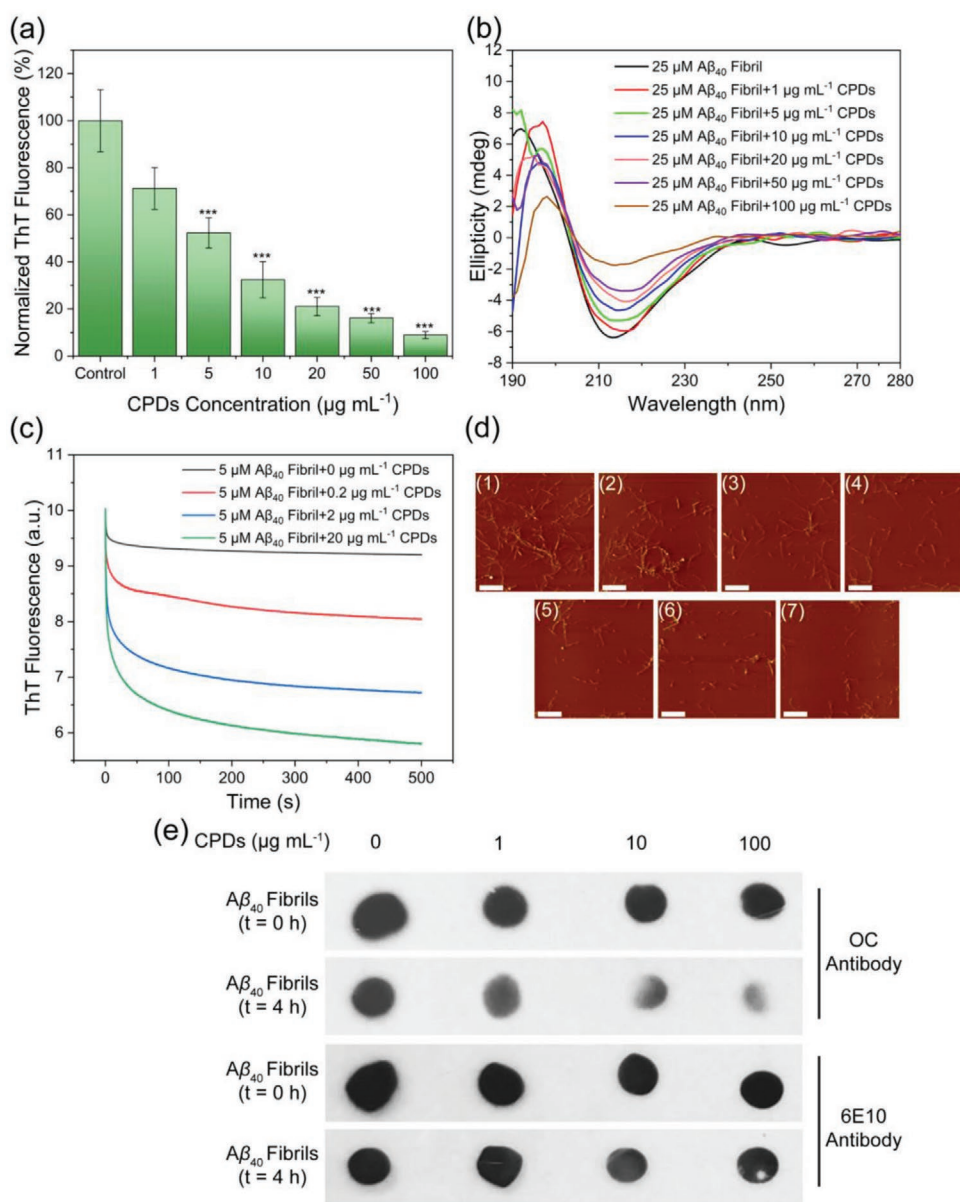
Figure 3. Disaggregation of Aβ_{40} fibrils by CPDs. a) Relative ThT fluorescence intensity and b) Far-UV circular dichroism spectra of Aβ_{40} fibrils incubated with CPDs (0–100 µg mL^{-1}) after 4 h at 37 °C. *** ($p < 0.001$) as compared to the control group. Error bars in graph represent the mean ± SD ($n = 3$). c) Fast disaggregation of Aβ_{40} fibrils by CPDs monitored by ThT fluorescence using a stopped-flow spectrometer in 500 s. d) AFM images of Aβ_{40} fibrils (aggregates) after co-incubation with CPDs (100 µg mL^{-1}) for 0 min (d1), 5 min (d2), 10 min (d3), 15 min (d4), 30 min (d5), 1 h (d6), and 4 h (d7). Scale bar, 2 µm. e) Dot-blot assay of disaggregation. Aβ_{40} fibrils (25 µM) was incubated with CPDs (1, 10, and 100 µg mL^{-1}). The samples were spotted onto nitrocellulose membrane, and probed with OC antibody and 6E10 antibody.

nanosheet could disassemble the preformed Aβ-Cu^{2+} aggregates in 4 h, and graphene oxide/graphitic carbon nitride (GO/g-C$_3$N$_4$) could photodegrade the aggregates of Aβ(33-42) under UV after 100 min incubation.[63,64] Hydroxylated single-walled carbon nanotubes (SWCN-OH) significantly remodeled the Aβ_{42} fibrils into small granular aggregates with the treatment for 5 h.[65] Photoactivated branched polyethylenimine-coated carbon nanodots (bPEI@CDs) distinctly facilitated the dissolution and disruption of β-sheet-rich Aβ fibrils to soluble species in 2 d.[66] Compared with the above literature data, CPDs significantly disintegrated the long and dense β-sheet rich Aβ fibrils to amorphous aggregates in 10 min, showing a high potency in the disassembly of preformed Aβ fibrils in a time scale of seconds to minutes (Figure 3c). We speculate that electrostatic interactions, H-bonding and hydrophobic interactions by the positively charged free amino groups and the skeleton of conjugated aromatic structures composed of pyrimidine rings, pyrrole rings, and benzene rings are the keys to the rapid remodeling potency of CPDs.

2.4. Fluorescent Imaging of $A\beta_{40}$ Aggregates by CPDs

The diagnosis of AD is mainly based on the assessment of the patient's cognitive status, which means that the disease is usually already in an advanced stage.[67,68] Current diagnostic criteria for AD recommend clinical and biomarker evidence to identify the different phases.[69] Therefore, it is a promising and effective strategy for early diagnosis of AD by determining the biomarker $A\beta$ deposition level in CSF.[70,71] Red emissive CPDs with the capabilities to inhibit $A\beta$ fibrillization and to remodel $A\beta$ fibrils are thus examined for the early diagnosis and therapy of AD. CPDs (100 µg mL^{-1}) have no green or red fluorescence in the absence of $A\beta_{40}$ (Figure S9, Supporting Information). Numerous and evident green fluorescent spots of ThT-$A\beta_{40}$

aggregates were observed after incubating $A\beta_{40}$ monomers and ThT for 56 h, demonstrating the formation of $A\beta$ fibrils (**Figure 4**a). Green fluorescence signals from ThT-labeled $A\beta_{40}$ aggregates decreased with the increase of CPDs concentration due to the inhibition effect of CPDs (Figure 4a,c,e,g), which was in agreement with the above inhibition results shown in Figure 2. Interestingly, interactions between CPDs and $A\beta_{40}$ aggregates resulted in distinct red fluorescence plaques (Figure 4d,f,h), whose distributions were consistent with those of green fluorescence (ThT) in Figure 4c,e,g. These fluorescent images indicate that CPDs not only inhibited $A\beta$ fibrillization but also bound to $A\beta_{40}$ to emit significant fluorescence like ThT. As compared to ThT, the red fluorescence is considered more favorable for in vivo imaging.[72,73]
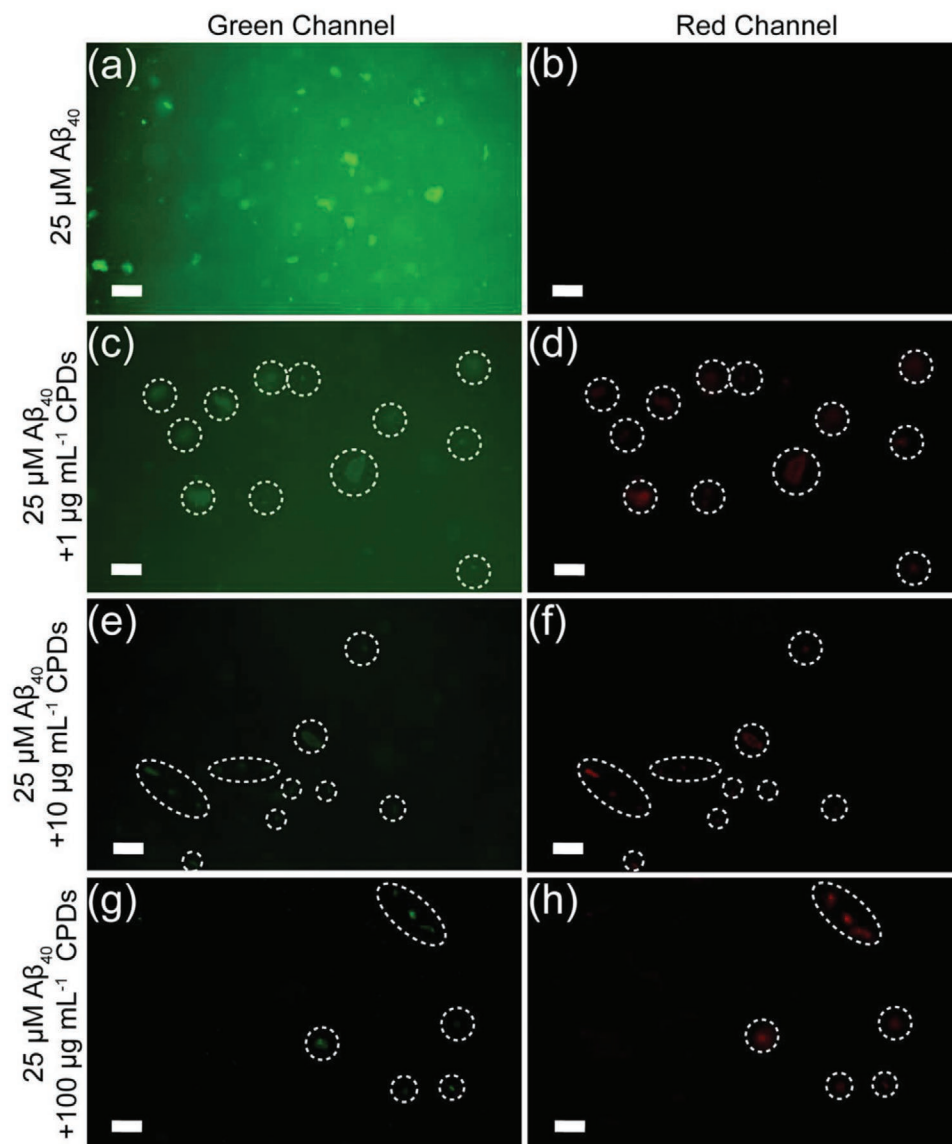

Figure 4. Fluorescence images of $A\beta_{40}$ incubated with or without CPDs after 56 h at 37 °C. 25 µM $A\beta_{40}$ with a,b) 0; c,d) 1; e,f) 10; and g,h) 100 µg mL^{-1} CPDs were observed by ThT and CPDs fluorescence, respectively. Left column recorded on excitation at 470/40 nm with a long-pass emission filter at 520 nm (Green Channel, ThT); right column recorded on excitation at 535/50 nm with a long-pass emission filter at 590 nm (Red Channel, CPDs). Scale bars, 100 µm.
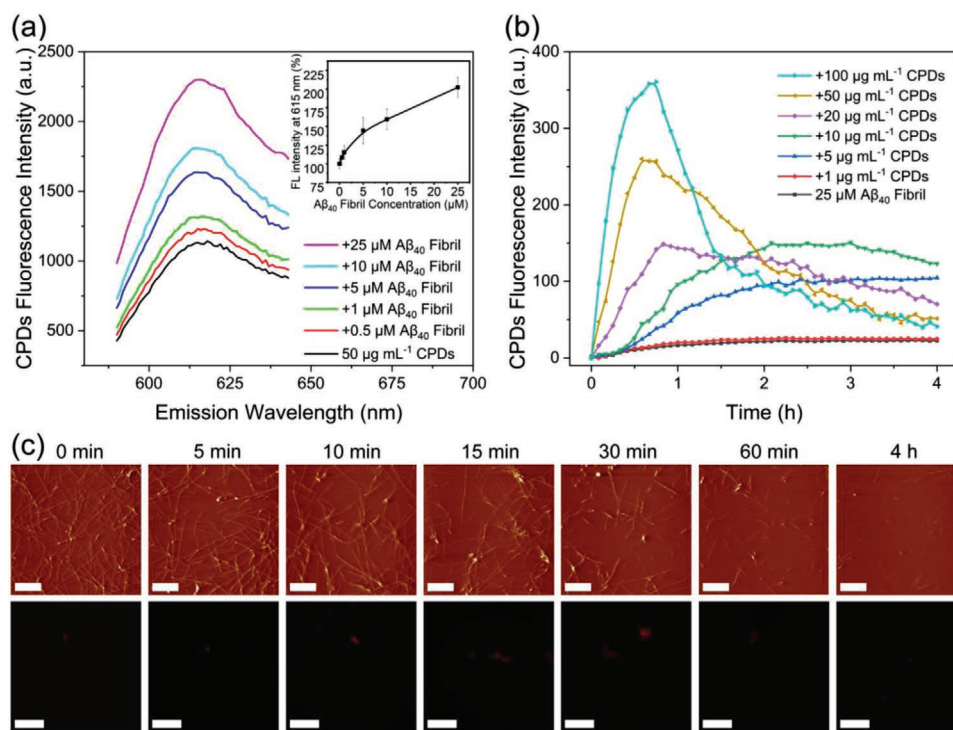
**ADVANCED
SCIENCE NEWS**

www.advancedsciencenews.com

NANO · MICRO

small

www.small-journal.com

Figure 5. Detection and the dynamics of disaggregation of $A\beta_{40}$ fibrils by using CPDs. a) Fluorescence spectra of CPDs (50 µg mL^{-1}) at different $A\beta_{40}$ fibril concentrations. Inset: Fluorescence intensities of CPDs (50 µg mL^{-1}) as a function of $A\beta_{40}$ fibril concentration (0–25 µM). Error bars in graph represent the mean ± SD (n = 3). b) Time-dependent CPDs fluorescence intensity of 25 µM $A\beta_{40}$ fibrils incubated with different CPDs concentrations (0–100 µg mL^{-1}) recorded on excitation at 560 nm and emission at 627 nm. c) AFM and fluorescence images of 25 µM $A\beta_{40}$ fibrils incubated with 50 µg mL^{-1} CPDs at different time intervals. The scale bars for AFM and fluorescence images are 2 and 100 µm, respectively.

As shown in **Figure 5**a, CPDs presented an increased emission upon binding to $A\beta_{40}$ fibrils, and its intensity at 615 nm increased in a nonlinear way with increasing the concentration of $A\beta_{40}$ fibrils. A slight blue-shift in the emission of CPDs was observed after interacting with $A\beta_{40}$ fibrils (Figure S10, Supporting Information), indicating the polarity reduction of the chromophores in microenvironment by binding to $A\beta_{40}$ fibrils.[74] This result indicates that $A\beta_{40}$ fibrils bound onto the CPDs surfaces/borders by electrostatic interactions, H-bonding and hydrophobic interactions via the amino groups and conjugated aromatic π system of CPDs. The non-covalent interactions could cause a rigid entanglement, limiting the molecular vibration and rotation, and thereby facilitating the red emission.[37,75–77]

To further clarify the potential of CPDs as a theranostic agent for remodeling and monitoring $A\beta_{40}$ fibrils, the fluorescence kinetics of CPDs was recorded and analyzed during the co-incubation with $A\beta_{40}$ fibrils. As illustrated in Figure 5b, at low CPDs concentrations (1–10 µg mL^{-1}), CPDs intensity gradually increased to a platform and remained stable for a while till starting decrease (which can be seen at 10 µg mL^{-1}). The result implies that CPDs could label $A\beta_{40}$ fibrils, but could not effectively disaggregate mature fibrils at low concentrations, consistent with the AFM images of disaggregation in Figure S7, Supporting Information. When CPDs concentrations were set to higher than 10 µg mL^{-1}, CPDs fluorescence intensity raised rapidly to a maximum in 35 to 50 min and then decreased with further incubation. The first phase of increased CPDs

fluorescence intensity is supposed to be a dynamic process where CPDs labeled $A\beta_{40}$ fibrils and disrupted mature fibrils simultaneously. The falling phase was attributed to the disaggregation of $A\beta_{40}$ fibrils by CPDs, in which most of the fibrils had been bound to CPDs. The AFM and fluorescence images observed at 50 µg mL^{-1} confirmed that long and dense $A\beta_{40}$ fibrils were finally disrupted by CPDs (Figure 5c, top panel), and the fluorescence signal of CPDs-fibrils increased and reached the maximum about 30 min, then gradually decreased and vanished (Figure 5c, bottom panel), which is in good agreement with that in Figure 5b. It is considered that the critical factor for CPDs to remove and detect $A\beta$ plaques is the unique structure with nitro, amino, pyrimidine rings, pyrrole rings, and benzene rings. The amino groups make CPDs positively charged in the physiological environment, and the conjugated aromatic rings provide hydrophobic binding sites, both of which would contribute to the elimination of $A\beta$ plaques via electrostatic, H-bonding, and hydrophobic interactions. Meanwhile, the electron-withdrawing groups (-NO$_2$) and the electron-donating groups (-NH$_2$) form a conjugated system with the CPDs skeleton to provide red fluorescence for the detection of $A\beta$ plaques.[28] These results demonstrate that CPDs had potent capabilities of fluorescence detection/imaging and removing of $A\beta_{40}$ fibrils, acting as a "scout" and "scavenger" of $A\beta$ plaques, which suggests the potential of CPDs for AD theranostics.

The above results indicate that the enhanced red fluorescence of CPDs by binding to $A\beta$ fibrils benefited in $A\beta$ detection and imaging. This CEE property has not been reported in
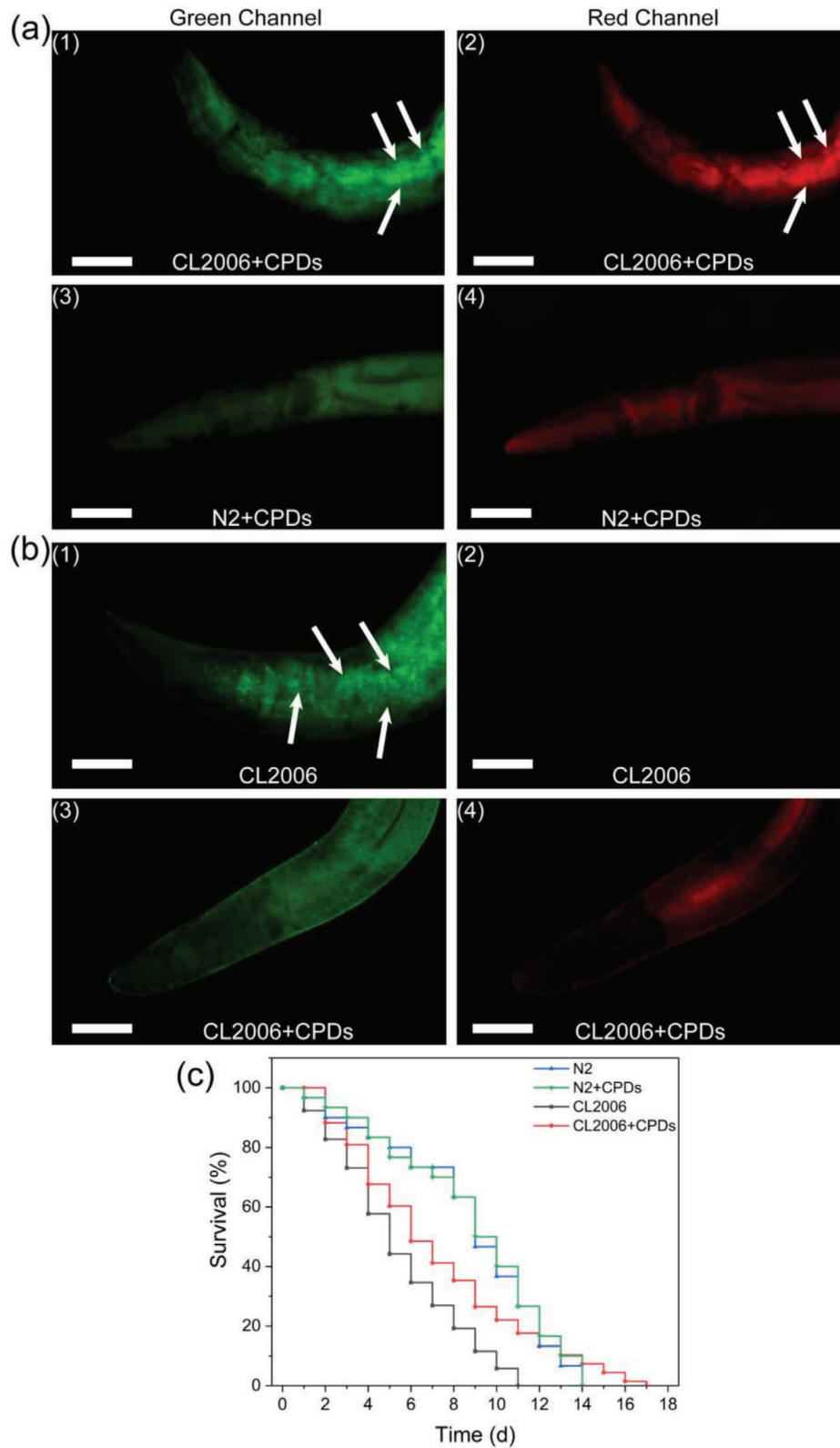
Figure 6. In vivo assays with *C. elegans* (CL2006 and N2). a) Fluorescence images of CL2006 (a1,a2) and N2 (a3,a4) nematodes co-stained with ThT and CPDs. b) Fluorescent images of inhibiting Aβ deposits after treating without (b1,b2) or with (b3,b4) CPDs in CL2006 nematodes. The experimental group and control group were stained with ThT under the same conditions. ThT fluorescence was excited at 470/40 nm and with long-pass emission filter at 520 nm (Green Channel, left column); CPDs fluorescence was excited at 535/50 nm and with long-pass emission filter at 590 nm (Red Channel, right column). Scale bars represent 50 μm. c) Survival curves of CL2006/N2 nematodes incubated with or without CPDs.

previous agents targeting Aβ aggregates. ThT shows enhanced fluorescence when binding to amyloid fibrils, but it has weak effect on Aβ fibrillization, so it is usually used as a fluorescence probe to quantify the β-sheet structures of amyloid fibrils.[78] Other agents or Aβ probes, such as quantum dot-poly(ethylene glycol)-benzotriazole (QD-PEG-BTA), graphitic carbon nitride quantum dot (gCNQD)-based fluorescent probe, and near-infrared fluorescence probes, can display excellent detection abilities for Aβ monomers or fibrils, but they have not either inhibiting or disaggregating capabilities for amyloidosis.[79–81] Thus, with the potencies of inhibiting Aβ fibrillogenesis, rapidly disaggregating mature Aβ fibrils, and CEE, CPDs exhibited scavenging and detecting capabilities targeting Aβ fibrillogenesis. The multifunctionality will be demonstrated in vivo in the following section.

2.5. *Caenorhabditis Elegans* Assays

C. elegans, as an in vivo model, is often used in studies of AD and other neurodegenerative diseases.[82] CL2006 expresses Aβ_{42} in body wall muscles constitutively,[17,83,84] so in vivo experiments were performed with it for evaluating the feasibility of CPDs for scavenging and imaging Aβ deposits in the nematodes as well as the effects of CPDs on the lifespan of the nematodes.

As shown in **Figure 6**, evident amyloid plaques labeled with ThT (green fluorescent spots in Figure 6-a1) and CPDs (red fluorescent spots in Figure 6-a2) can be seen in adult CL2006 nematodes after staining with ThT and CPDs, respectively. As a control, no such fluorescent spots were observed in the wild-type nematodes (N2) that did not express Aβ (Figure 6-a3,a4). This result demonstrates the effectiveness of CPDs for in vivo imaging of Aβ plaques.

Then, to validate the capabilities of CPDs for inhibiting Aβ accumulation in nematodes, CL2006 nematodes were administrated with 100 µg mL^{-1} CPDs at the L4 larval stage and cultured for 3 d. ThT staining images showed the amyloid aggregation in the untreated CL2006, as presented by the scattered green fluorescence spots in Figure 6-b1, whereas there were no amyloid plaques in the CL2006 nematodes with CPDs treatment (Figure 6-b3,b4), illustrating the inhibition of Aβ_{42} plaques formation in CL2006. In addition, the red fluorescence of CPDs in CL2006 can be seen (Figure 6-b4), indicating that CPDs mainly accumulated in the intestinal lumen of the nematode.

In the lifespan assay, CPDs showed no significant effect on the lifespan of the wild-type N2 nematodes, confirming its good biocompatibility. The untreated CL2006 nematodes completely paralyzed and died within 11 d, while CPDs treatment attenuated Aβ-induced toxicity and postponed the complete death to 17 d (Figure 6c). The lifespan increase was comparable to or superior over those with other nano-agents, such as Hf-metal–organic frameworks (Hf-MOFs), BP@BTA (BP: black phosphorus, BTA: 4-(6-methyl-1,3-benzothiazol-2-yl)phenylamine), and UCNP@C$_{60}$-pep (UCNP: upconversion nanoparticle, pep: Aβ-target peptide KLVFF),[17,85,86] which extended lifespan of CL2006 strain by 3, 4, and 5 days, respectively. The results demonstrated the potential of CPDs as a potent in vivo scavenger and detector targeting the Aβ_{42} deposits.

3. Conclusions

In this work, we have found the multifunctionality of N-doped carbonized polymer dots, CPDs, for targeting Aβ aggregation, and toxicity. Based on the results of ThT, AFM, CD, and immunoassays, it is reasonable to speculate that CPDs could effectively modulate Aβ aggregation, scavenge Aβ mature fibrils in a time scale of seconds to minutes, and form off-pathway Aβ species via electrostatic interactions, H-bonding, and hydrophobic interactions. The multiple interactions between the positively charged amino groups of CPDs and the negatively residuals of Aβ, and between the conjugated aromatic π system of CPDs and the hydrophobic core of Aβ are considered to be the main factors for preventing the conformational transition of Aβ to β-sheet-rich structures and label Aβ aggregates through crosslink-enhanced emission. The Aβ scavenging and detecting capabilities of CPDs was proven by in vivo assays with *C. elegans* CL2006, indicating its promise for AD theranostics. This work may provide vital enlightenment for the application of carbon nanomaterials in the treatment and diagnosis of neurodegenerative diseases as well as other protein conformational diseases.

4. Experimental Section

Materials: o-Phenylenediamine, thioflavin T (ThT), 1,1,1,3,3,3-hexafluoro-2-propanol (HFIP), 3-(4,5-dimethylthiazol-2-yl)-2,5-diphenyltetrazolium bromide (MTT), 4-(2-hydroxyethyl)-1-piperazineethanesulfonic acid (HEPES), and dimethyl sulfoxide (DMSO) were purchased from Sigma (St. Louis, MO, USA). Aβ_{40} (>95.0%, lyophilized powder), synthesized by routine solid-phase peptide synthesis and Fmoc chemistry, were purchased from Ziyu peptide Inc (Shanghai, China). Human neuroblastoma SH-SY5Y cells were obtained from the Cell Bank of the Chinese Academy of Sciences (Shanghai, China). Fetal bovine serum (FBS) and Dulbecco's modified Eagle medium/Ham's F-12 (DMEM/F12) were obtained from Invitrogen (Carlsbad, CA, USA). Antibodies and kits used in the dot-blot assays included: rabbit polyclonal anti-amyloid fibrils OC antibody (AB2286, Merck); mouse monoclonal anti-Aβ_{1-16} 6E10 antibody (803014, Biolegend); rabbit polyclonal anti-amyloid oligomers A11 antibody (ab126892, Abcam); horseradish peroxidase-conjugated goat anti-rabbit IgG (H+L) (IH-0011, Dingguo Biotech); horseradish peroxidase-conjugated goat anti-mouse IgG (H+L) (A0216, Beyotime); and hypersensitive ECL chemiluminescence kit (P0018S, Beyotime). The wild-type N2 strain and the transgenic CL2006 strain were purchased from the Caenorhabditis Genetics Center, CGC (University of Minnesota, MN, USA). All other reagents were of analytical grade and purchased from local sources. Deionized water filtered through 0.22 µm filters was used for all solution preparations.

Synthesis of CPDs: CPDs were synthesized by one-step hydrothermal treatment according to Yang's work.[28] First, o-phenylenediamine (54.07 mg, 0.5 mmol) and HNO$_3$ (50 µL, 0.725 mmol) were dissolved in deionized water (10 mL). Then, the solution was transferred to a poly(tetrafluoroethylene)-lined autoclave (25 mL) and heated in a 200 °C furnace for 10 h. After the reactor was cooled to room temperature, the CPDs solution was dialyzed with deionized water in a 500 Da dialysis bag for 24 h and dialyzed with ethanol for another 24 h. The solution was filtered through a 0.22 µm nylon membrane to remove large particles of CPDs in ethanol. Black powder of CPDs was obtained by rotary evaporation to remove the solvent and stored at 4 °C before use.

Characterization of CPDs: The morphology and size distribution of CPDs were recorded with a field emission transmission electron microscope (JEM-2100F, JEOL, Japan). XPS was detected by an X-ray

**ADVANCED
SCIENCE NEWS**

www.advancedsciencenews.com

**NANO · MICRO
small**

www.small-journal.com

photoelectron spectrometer (ESCALAB 250Xi, Thermo Fisher, USA) with a mono X-ray source Al Kα excitation (1486.6 eV). Fourier transform infrared spectra (FTIR) were measured with a Fourier transform infrared spectrometer (Nicolet 6700, Thermo Fisher, USA), using the KBr tablet method to prepare samples. The fluorescence spectra were scanned with a fluorescence spectrometer (LS55, PerkinElmer, USA). ζ potential was conducted using a Zetasizer (Nano ZS, Malvern, UK).

Preparation of Aβ40 Monomer/Fibril Solution: Aβ40 monomer solution was prepared as described in the literature.[87] Briefly, Aβ40 powder was dissolved in HFIP to 1.0 mg mL^{-1}. Then, the solution was placed at 4 °C for 2 h and sonicated in ice bath for 30 min to destroy the pre-existing Aβ40 fibrils. HFIP was then removed with a vacuum freeze drier (Labconco, MO, USA). The lyophilized Aβ40 was stored at -20 °C immediately. Before use, the treated Aβ40 was dissolved in 20 mM NaOH at 275 or 550 μM and sonicated in ice bath for 10 min to ensure that Aβ40 is completely dissolved. After centrifugation at 16 000g for 20 min at 4 °C, 75.0% of the supernatant was carefully collected as Aβ40 stock solution for subsequent use. In the inhibition of Aβ40 aggregation and corresponding cell experiments, 275 μM Aβ40 stock solution was added to HEPES buffer (20 mM HEPES, 100 mM NaCl, pH = 7.4) with different concentrations of CPDs to make the final Aβ40 concentration of 25 μM. In the experiments of disaggregating Aβ40 fibrils, 550 μM Aβ40 stock solution was diluted with HEPES buffer or PBS buffer (100 mM sodium phosphate, 10 mM NaCl, pH = 7.4) to 50 μM, and then cultured at 37 °C for 3 days to obtain pre-prepared mature Aβ40 fibrils. The pre-prepared Aβ40 fibrils solution was then added to HEPES buffer or PBS buffer with different concentrations of CPDs to the final concentration of 25 μM.

Thioflavin T Fluorescence Assay: ThT fluorescence experiments were performed using a microplate reader (TECAN Infinite, Salzburg, Austria). Samples (200 μL in HEPES buffer) containing 25 μM Aβ40 monomers/fibrils, 25 μM ThT, and different concentrations of CPDs were mixed in a 96-well plate and continuously cultured at 37 °C. The fluorescence intensity was measured with excitation at 440 nm and emission at 480 nm, 10 min reading intervals, and 5 s shaking before each read until ThT fluorescence reached the plateau phase. For the aggregation experiment, the sigmoidal kinetic aggregation curves were normalized and fitted using the following equation:

$$y = y_0 + \frac{y_{max} - y_0}{1 + e^{-(t-t_{1/2})k}} \tag{1}$$

where y is the ThT fluorescence intensity at time t; y_0 and y_{max} are the minimum and maximum ThT fluorescence intensities, respectively; $t_{1/2}$ is the time when the ThT fluorescence intensity reaches 50.0% of maximum ThT fluorescence intensity; and k is the elongation rate constant. The lag time (T_{lag}) was then calculated from Equation (2).[88]

$$T_{lag} = t_{1/2} - \frac{2}{k} \tag{2}$$

Fluorescence Microscopy: Monomeric Aβ40 or Aβ40 fibrils (25 μM) was incubated with or without CPDs (1, 10, and 100 μg mL^{-1}) in HEPES buffer at 37 °C. The samples were observed with an inverted fluorescence microscope (TE2000-U, Nikon, Japan) at different intervals.

Stopped-Flow Fluorescent Spectroscopy: The rapid disaggregation of Aβ40 fibrils by CPDs was studied using a stopped-flow spectrometer (SX20, Applied Photophysics, UK) on a time scale of seconds. The protein solution of 55 μM Aβ40 fibrils containing 55 μM ThT and the CPDs solution of 0.22-22 μg mL^{-1} were quickly mixed in a volume ratio of 1:10 at 37 °C. ThT fluorescence intensity at 480 nm was recorded with excitation at 440 nm.

AFM: The morphology of Aβ40 aggregates was observed with an atomic force microscope (CSPM5500, Benyuan, China) in a tapping mode. In the inhibition of aggregation experiments, Aβ40 monomer solutions (25 μM) with different concentrations of CPDs were incubated at 37 °C for 56 h. 100 μL sample was then deposited on a freshly stripped mica flake for 5 min, rinsed with ultrapure water to remove salts in the sample, and finally dried using a spin coater (KW-A4, IMECAS, China)

at 1000 rpm for 60 s. In the disaggregation experiments, 25 μM Aβ40 mature fibrils with different concentrations of CPDs were incubated at 37 °C and 150 rpm in a shaker. Then, 100 μL sample was taken out at 0, 5, 10, 15, 30, 60 min, and 4 h, respectively, and prepared in the same way as above.

CD Spectroscopy: The effects of CPDs on the secondary structure of Aβ40 aggregates were investigated using a circular dichroism spectrometer (J-810, Jasco, Japan). For the samples of aggregation, a freshly prepared Aβ40 stock solution was diluted in PBS buffer (100 mM sodium phosphate, 10 mM NaCl, pH = 7.4) with different concentrations of CPDs to a final concentration of 25 μM, then incubated in a 150 rpm shaker at 37 °C for 72 h. For the samples of disaggregation, a pre-prepared Aβ40 fibrils solution (50 μM) was diluted in PBS buffer with different concentrations of CPDs to the desired concentration (25 μM), and the samples were incubated in a 150 rpm shaker at 37 °C for 4 h. The ellipticity was recorded in the spectral range 190–260 nm using a 1 mm path length quartz cell at a scanning speed of 100 nm min^{-1} and a bandwidth of 1 nm. All far-UV CD spectra of each sample were the average of three consecutive scans.

Cell Viability Assay: MTT assays were used to determine the cell viability with SH-SY5Y cells. SH-SY5Y cells were cultured in DMEM/F12 medium containing 20.0% FBS, 1.0% penicillin–streptomycin antibiotic (100 U mL^{-1} penicillin and 100 U mL^{-1} streptomycin), at 37 °C, 5.0% CO$_2$ in a cell incubator. 8×10^3 cells well^{-1} (80 μL) was added to a sterile 96-well plate and cultured for 24 h. Aβ40 was aged with or without CPDs in a 150 rpm shaker at 37 °C for 24 h. Then, 20 μL of aged Aβ40 solutions (25 μM) was added into the 96-well plate and incubated for an additional 24 h. After that, 10 μL MTT (5.5 μg mL^{-1}) in HEPES buffer was added to each well and cultured for 4 h. The culture medium was removed after centrifuging the suspension of 96-well plate at 1500 rpm for 10 min. The precipitated cells were lysed by 100 μL DMSO in each well and shaken at 37 °C for 20 min to dissolve formazan completely. The absorbance at 570 nm was measured with a microplate reader. The sample of each group was carried out with six replicates. All the experimental values were obtained by subtracting the background signals of the medium without cells. The cells treated with HEPES buffer were set as control, and other treated groups were normalized. The cell viability was estimated according to the following equation:

$$\text{Cell viability (\%)} = \frac{100\% \times (OD_{Treated} - OD_{Background})}{OD_{Control} - OD_{Background}} \tag{3}$$

where $OD_{Treated}$ was obtained in the presence of CPDs.

Dot-Blot Assay: Aβ40 monomers (25 μM) or fibrils (25 μM) were incubated for the initial and final time points in the absence or presence of CPDs (1, 10, and 100 μg mL^{-1}) and kept at −80 °C until analyzed. Samples (10 μL for OC or 6E10 experiments; 10 μL × 8 times for A11 experiments) were then spotted onto nitrocellulose membranes (0.2 μM) and dried at room temperature. The membranes were then blocked with 10.0% skim milk in Tris-buffered saline (TBS) (20 mM Tris-HCl, 150 mM NaCl, pH = 7.4) containing 0.05% Tween 20 (TBST) at 4 °C for 12 h, washed with TBST (3 × 5 min), and incubated with the primary antibody OC (for amyloid fibrils, 1:3000), 6E10 (for all forms of Aβ species, 1:5000) or A11 (for amyloid oligomers, 1:2000) in TBST at 4 °C for 12 h. After three washes with TBST (3 × 5 min), the membranes were incubated with appropriate horseradish peroxidase-labeled secondary antibodies (Goat Anti-Rabbit IgG, 1:5000; Goat Anti-Mouse IgG, 1:1000) for 1 h at room temperature, washed with TBST (3 × 5 min) to remove unbound secondary antibody, and finally developed with an ECL chemiluminescence kit.

CPDs Fluorescence Experiments: CPD (50 μg mL^{-1}) and Aβ40 fibrils at different concentrations were pre-incubated at 37 °C for 30 min; then, CPDs fluorescence spectra at 590–643 nm were recorded with a microplate reader with an excitation wavelength of 560 nm. In the disaggregation kinetics of Aβ40 fibrils, 25 μM Aβ40 fibrils were incubated with or without CPDs at 37 °C for 4 h, and CPDs fluorescence intensities at 627 nm were measured with excitation at 560 nm, 10 min reading intervals, and 5 s shaking.

C. Elegans Experiments: In this study, two kinds of nematodes were used, including the wild-type N2 strain and the transgenic CL2006 strain. The nematodes were cultured on solid nematode growth medium (NGM contains 3 g L^{-1} NaCl, 1 mm $CaCl_2$, 1 mm $MgSO_4$, 17 g L^{-1} agar, 2.5 g L^{-1} peptone, 250 mm KH_2PO_4, pH 6.0) plates seeded with *E. coli* OP50 as food resources in an incubator at 20 °C.

For in vivo imaging of $A\beta_{42}$ deposits in N2 and CL2006 nematodes, adult N2 and CL2006 nematodes were, respectively, collected and fixed by 4.0% paraformaldehyde at 4 °C for 24 h. Then, the fixed nematodes were washed with deionized water and stained with 100 µg mL^{-1} CPDs and 10 µm ThT in HEPES buffer for another 4 h, followed by washing with deionized water and observation with an inverted fluorescence microscope.

For CPDs inhibiting $A\beta_{42}$ deposits in CL2006 nematodes, the L4 larvae were transferred onto fresh NGM plates containing *E. coli* OP50 with or without CPDs (100 µg mL^{-1}, 300 µL). When CL2006 nematodes grew up to adult for 3d, they were collected and fixed by 4.0% paraformaldehyde at 4 °C for 24 h. Then, 4.0% paraformaldehyde was removed by centrifuging 2 min at 1200 rpm. The nematodes were washed 3 times with deionized water and stained with 10 µm ThT for 4 h. Then, the stained nematodes were washed 3 times, mounted on glass slides, and observed with an inverted fluorescence microscope.

For lifespan assay, 50 N2 or CL2006 nematodes at L4 larval stage were transferred onto fresh NGM plates with or without CPDs (100 µg mL^{-1}, 300 µL), and 300 µL of 150 µm fluorodeoxyuridine (FUDR) was added to plates to sterilize the nematodes. The number of surviving nematodes was counted every 24 h until all nematodes were scored as dead or censored. Each group of survivors was transferred onto fresh NGM plate containing *E. coli* OP50 with or without CPDs every 3 days. The nematodes were recognized as dead when they did not move after gentle touches with a platinum wire.

Statistical Analysis: All data were expressed as mean ± SD. Statistical analyses were determined using a one-way analysis of variance (ANOVA) followed by a statistical comparison using Tukey test. Statistical significance was expressed as * $p < 0.05$, ** $p < 0.01$, and *** (###) $p < 0.001$.

Supporting Information

Supporting Information is available from the Wiley Online Library or from the author.

Conflict of Interest

The authors declare no conflict of interest.

[1] F. Torreilles, J. Touchon, *Prog. Neurobiol.* **2002**, *66*, 191.
[2] M. P. Mattson, *Nature* **2004**, *430*, 631.
[3] P. Scheltens, K. Blennow, M. M. B. Breteler, B. de Strooper, G. B. Frisoni, S. Salloway, W. M. Van der Flier, *Lancet* **2016**, *388*, 505.
[4] A. Burns, S. Iliffe, *BMJ* **2009**, *338*, 467.
[5] M. V. F. Silva, C. M. G. Loures, L. C. V. Alves, L. C. de Souza, K. B. G. Borges, M. D. G. Carvalho, *J. Biomed. Sci.* **2019**, *26*, 33.
[6] W. Zheng, M. Y. Tsai, P. G. Wolynes, *J. Am. Chem. Soc.* **2017**, *139*, 16666.
[7] D. J. Selkoe, J. Hardy, *EMBO Mol. Med.* **2016**, *8*, 595.
[8] J. Hardy, D. J. Selkoe, *Science* **2002**, *297*, 353.
[9] F. Yang, G. P. Lim, A. N. Begum, O. J. Ubeda, M. R. Simmons, S. S. Ambegaokar, P. P. Chen, R. Kayed, C. G. Glabe, S. A. Frautschy, G. M. Cole, *J. Biol. Chem.* **2005**, *280*, 5892.
[10] W. J. Du, J. J. Guo, M. T. Gao, S. Q. Hu, X. Y. Dong, Y. F. Han, F. F. Liu, S. Jiang, Y. Sun, *Sci. Rep.* **2015**, *5*, 7992.
[11] Y. Liu, Y. Liu, S. Wang, S. Dong, P. Chang, Z. Jiang, *RSC Adv.* **2015**, *5*, 62402.
[12] W. Liu, X. Dong, Y. Sun, *ACS Chem. Neurosci.* **2019**, *10*, 1390.
[13] M. Richman, S. Wilk, M. Chemerovski, S. K. Warmlander, A. Wahlstrom, A. Graslund, S. Rahimipour, *J. Am. Chem. Soc.* **2013**, *135*, 3474.
[14] J. Luo, S. K. Warmlander, A. Graslund, J. P. Abrahams, *Chem. Commun.* **2013**, *49*, 6507.
[15] W. Wang, X. Dong, Y. Sun, *Bioconjugate Chem.* **2019**, *30*, 1477.
[16] N. Xiong, Y. Zhao, X. Dong, J. Zheng, Y. Sun, *Small* **2017**, *13*, 1601666.
[17] Z. Du, N. Gao, X. Wang, J. Ren, X. Qu, *Small* **2018**, *14*, 1801852.
[18] E. de la Fuente, C. Adura, M. J. Kogan, S. Bollo, *Electroanalysis* **2012**, *24*, 938.
[19] M. Li, X. Yang, J. Ren, K. Qu, X. Qu, *Adv. Mater.* **2012**, *24*, 1722.
[20] H. Jung, Y. J. Chung, R. Wilton, C. H. Lee, B. I. Lee, J. Lim, H. Lee, J. H. Choi, H. Kang, B. Lee, E. A. Rozhkova, C. B. Park, J. Lee, *Adv. Funct. Mater.* **2020**, *30*.
[21] P. C. Ke, E. H. Pilkington, Y. Sun, I. Javed, A. Kakinen, G. Peng, F. Ding, T. P. Davis, *Adv. Mater.* **2020**, *32*, 1901690.
[22] H. Huang, P. Li, M. Zhang, Y. Yu, Y. Huang, H. Gu, C. Wang, Y. Yang, *Nanoscale* **2017**, *9*, 5044.
[23] S. Xiao, D. Zhou, P. Luan, B. Gu, L. Feng, S. Fan, W. Liao, W. Fang, L. Yang, E. Tao, R. Guo, J. Liu, *Biomaterials* **2016**, *106*, 98.
[24] Y. Liu, L. P. Xu, W. Dai, H. Dong, Y. Wen, X. Zhang, *Nanoscale* **2015**, *7*, 19060.
[25] M. Wang, Y. Sun, X. Cao, G. Peng, I. Javed, A. Kakinen, T. P. Davis, S. Lin, J. Liu, F. Ding, P. C. Ke, *Nanoscale* **2018**, *10*, 19995.
[26] M. Yousaf, H. Huang, P. Li, C. Wang, Y. Yang, *ACS Chem. Neurosci.* **2017**, *8*, 1368.
[27] D. Kim, J. M. Yoo, H. Hwang, J. Lee, S. H. Lee, S. P. Yun, M. J. Park, M. Lee, S. Choi, S. H. Kwon, S. Lee, S. H. Kwon, S. Kim, Y. J. Park, M. Kinoshita, Y. H. Lee, S. Shin, S. R. Paik, S. J. Lee, S. Lee, B. H. Hong, H. S. Ko, *Nat. Nanotechnol.* **2018**, *13*, 812.
[28] J. Liu, D. Li, K. Zhang, M. Yang, H. Sun, B. Yang, *Small* **2018**, *14*, 1703919.
[29] Y. Liu, J. Liu, J. Zhang, X. Li, F. Lin, N. Zhou, B. Yang, L. Lu, *ACS Omega* **2018**, *3*, 7888.
[30] C. Xia, S. Zhu, T. Feng, M. Yang, B. Yang, *Adv. Sci.* **2019**, *6*, 1901316.
[31] F. Hu, Y. Huang, G. Zhang, R. Zhao, H. Yang, D. Zhang, *Anal. Chem.* **2014**, *86*, 7987.
[32] T. Han, X. Gu, J. W. Y. Lam, A. C. S. Leung, R. T. K. Kwok, T. Han, B. Tong, J. Shi, Y. Dong, B. Z. Tang, *J. Mater. Chem. C* **2016**, *4*, 10430.
[33] X. Tan, Y. Li, X. Li, S. Zhou, L. Fan, S. Yang, *Chem. Commun.* **2015**, *51*, 2544.
[34] H. Nie, M. Li, Q. Li, S. Liang, Y. Tan, L. Sheng, W. Shi, S. X.-A. Zhang, *Chem. Mater.* **2014**, *26*, 3104.
[35] L. Tang, R. Ji, X. Li, G. Bai, C. P. Liu, J. Hao, J. Lin, H. Jiang, K. S. Teng, Z. Yang, S. P. Lau, *ACS Nano* **2014**, *8*, 6312.
[36] U. Olgun, M. Gülfen, *React. Funct. Polym.* **2014**, *77*, 23.
[37] S. Tao, S. Zhu, T. Feng, C. Zheng, B. Yang, *Angew. Chem. Int. Ed. Engl.* **2020**, *59*, 9826.

[38] R. Cai, C. Chen, *Adv. Mater.* **2019**, *31*, 1805740.

[39] R. Khurana, C. Coleman, C. Ionescu-Zanetti, S. A. Carter, V. Krishna, R. K. Grover, R. Roy, S. Singh, *J. Struct. Biol.* **2005**, *151*, 229.

[40] M. Biancalana, S. Koide, *Biochim. Biophys. Acta* **2010**, *1804*, 1405.

[41] S. J. Wood, B. Maleeff, T. Hart, R. Wetzel, *J. Mol. Biol.* **1996**, *256*, 870.

[42] C. Cabaleiro-Lago, F. Quinlan-Pluck, I. Lynch, K. A. Dawson, S. Linse, *ACS Chem. Neurosci.* **2010**, *1*, 279.

[43] X. Li, W. Wang, X. Dong, Y. Sun, *J. Mater. Chem. B* **2020**, *8*, 2256.

[44] G. Zhao, X. Dong, Y. Sun, *Langmuir* **2019**, *35*, 1846.

[45] A. C. Brorsson, J. R. Kumita, I. MacLeod, B. Bolognesi, E. Speretta, L. M. Luheshi, T. P. Knowles, C. M. Dobson, D. C. Crowther, *Front. Biosci., Landmark Ed.* **2010**, *15*, 373.

[46] H. Zhang, X. Dong, Y. Sun, *ACS Chem. Neurosci.* **2018**, *9*, 2689.

[47] R. Liu, H. Barkhordarian, S. Emadi, C. B. Park, M. R. Sierks, *Neurobiol. Dis.* **2005**, *20*, 74.

[48] B. Strohm, *Encyclopedia of Toxicology*, Elsevier, Troy, MI **2014**.

[49] B. J. Phillips, P. Jenkinson, *Mutagenesis* **2001**, *16*, 91.

[50] I. Javed, G. Peng, Y. Xing, T. Yu, M. Zhao, A. Kakinen, A. Faridi, C. L. Parish, F. Ding, T. P. Davis, P. C. Ke, S. Lin, *Nat. Commun.* **2019**, *10*, 3780.

[51] Y. Liu, L. P. Xu, Q. Wang, B. Yang, X. Zhang, *ACS Chem. Neurosci.* **2018**, *9*, 817.

[52] X. Han, Z. Jing, W. Wu, B. Zou, Z. Peng, P. Ren, A. Wikramanayake, Z. Lu, R. M. Leblanc, *Nanoscale* **2017**, *9*, 12862.

[53] Z. Liu, X. Li, X. Wu, C. Zhu, *J. Mater. Chem. B* **2019**, *7*, 1292.

[54] W.-T. Dou, Y. Lv, C. Tan, G.-R. Chen, X.-P. He, *J. Mater. Chem. B* **2016**, *4*, 4502.

[55] P. Ryan, B. Patel, V. Makwana, H. R. Jadhav, M. Kiefel, A. Davey, T. A. Reekie, S. Rudrawar, M. Kassiou, *ACS Chem. Neurosci.* **2018**, *9*, 1530.

[56] L. Jia, W. Zhao, J. Sang, W. Wang, W. Wei, Y. Wang, F. Zhao, F. Lu, F. Liu, *ACS Chem. Neurosci.* **2019**, *10*, 4696.

[57] C. Haass, D. J. Selkoe, *Nat. Rev. Mol. Cell Biol.* **2007**, *8*, 101.

[58] I. C. Martins, I. Kuperstein, H. Wilkinson, E. Maes, M. Vanbrabant, W. Jonckheere, P. Van Gelder, D. Hartmann, R. D'Hooge, B. De Strooper, J. Schymkowitz, F. Rousseau, *EMBO J.* **2008**, *27*, 224.

[59] J. Bieschke, J. Russ, R. P. Friedrich, D. E. Ehrnhoefer, H. Wobst, K. Neugebauer, E. E. Wanker, *Proc. Natl. Acad. Sci. U. S. A.* **2010**, *107*, 7710.

[60] F. L. Palhano, J. Lee, N. P. Grimster, J. W. Kelly, *J. Am. Chem. Soc.* **2013**, *135*, 7503.

[61] A. Kakinen, J. Adamcik, B. Wang, X. Ge, R. Mezzenga, T. P. Davis, F. Ding, P. C. Ke, *Nano Res.* **2018**, *11*, 3636.

[62] Q. Wang, X. Yu, K. Patal, R. Hu, S. Chuang, G. Zhang, J. Zheng, *ACS Chem. Neurosci.* **2013**, *4*, 1004.

[63] M. Li, Y. Guan, C. Ding, Z. Chen, J. Ren, X. Qu, *J. Mater. Chem. B* **2016**, *4*, 4072.

[64] J. Wang, Z. Zhang, H. Zhang, C. Li, M. Chen, L. Liu, M. Dong, *ACS Appl. Mater. Interfaces* **2019**, *11*, 96.

[65] F. Liu, W. Wang, J. Sang, L. Jia, F. Lu, *ACS Chem. Neurosci.* **2019**, *10*, 588.

[66] Y. J. Chung, K. Kim, B. I. Lee, C. B. Park, *Small* **2017**, *13*, 1700983.

[67] Z. Yang, M. J. Slavin, P. S. Sachdev, *Nat. Rev. Neurol.* **2013**, *9*, 382.

[68] K. Rajasekhar, N. Narayanaswamy, N. A. Murugan, K. Viccaro, H. G. Lee, K. Shah, T. Govindaraju, *Biosens. Bioelectron.* **2017**, *98*, 54.

[69] J. Cummings, *Alzheimers Res. Ther.* **2012**, *4*, 35.

[70] N. Toschi, S. Lista, F. Baldacci, E. Cavedo, H. Zetterberg, K. Blennow, I. Kilimann, S. J. Teipel, A. Melo Dos Santos, S. Epelbaum, F. Lamari, R. Genthon, M. O. Habert, B. Dubois, R. Floris, F. Garaci, A. Vergallo, H. Hampel, the INSIGHT-preAD study group for the Alzheimer Precision Medicine Initiative (APMI), *Neurobiol. Aging* **2019**, *83*, 42.

[71] L. C. Brazaca, I. Sampaio, V. Zucolotto, B. C. Janegitz, *Talanta* **2020**, *210*, 120644.

[72] H. Watanabe, M. Ono, H. Saji, *Chem. Commun.* **2015**, *51*, 17124.

[73] G. S. Filonov, K. D. Piatkevich, L. M. Ting, J. Zhang, K. Kim, V. V. Verkhusha, *Nat. Biotechnol.* **2011**, *29*, 757.

[74] J. R. Lakowicz, *Principles of Fluorescence Spectroscopy*, Springer, Boston, MA **2006**.

[75] Y. O. Lee, J. W. Shin, C. Yi, Y. H. Lee, N. W. Sohn, C. Kang, J. S. Kim, *Chem. Commun.* **2014**, *50*, 5741.

[76] P. Verwilst, H. R. Kim, J. Seo, N. W. Sohn, S. Y. Cha, Y. Kim, S. Maeng, J. W. Shin, J. H. Kwak, C. Kang, J. S. Kim, *J. Am. Chem. Soc.* **2017**, *139*, 13393.

[77] M. M. Xu, W. M. Ren, X. C. Tang, Y. H. Hu, H. Y. Zhang, *Acta Pharmacol. Sin.* **2016**, *37*, 719.

[78] C. Xue, T. Y. Lin, D. Chang, Z. Guo, *R. Soc. Open Sci.* **2017**, *4*, 160696.

[79] L. Quan, J. Wu, L. A. Lane, J. Wang, Q. Lu, Z. Gu, Y. Wang, *Bioconjugate Chem.* **2016**, *27*, 809.

[80] Y. Zhang, S. Meng, J. Ding, Q. Peng, Y. Yu, *Analyst* **2019**, *144*, 504.

[81] M. Cui, M. Ono, H. Watanabe, H. Kimura, B. Liu, H. Saji, *J. Am. Chem. Soc.* **2014**, *136*, 3388.

[82] A. G. Alexander, V. Marfil, C. Li, *Front. Genet.* **2014**, *5*, 279.

[83] M. Morita, K. Osoda, M. Yamazaki, F. Shirai, N. Matsuoka, H. Arakawa, S. Nishimura, *Brain Res.* **2009**, *1295*, 186.

[84] Y. Guan, Y. Du, N. Gao, Y. Cao, X. Wang, P. Scott, H. Song, J. Ren, X. Qu, *Sci. Adv.* **2018**, *4*, eaao6718.

[85] D. Yu, Y. Guan, F. Bai, Z. Du, N. Gao, J. Ren, X. Qu, *Chem. Eur. J.* **2019**, *25*, 3489.

[86] Y. Li, Z. Du, X. Liu, M. Ma, D. Yu, Y. Lu, J. Ren, X. Qu, *Small* **2019**, *15*, 1901116.

[87] Q. Wang, N. Shah, J. Zhao, C. Wang, C. Zhao, L. Liu, L. Li, F. Zhou, J. Zheng, *Phys. Chem. Chem. Phys.* **2011**, *13*, 15200.

[88] C. Cabaleiro-Lago, F. Quinlan-Pluck, I. Lynch, S. Lindman, A. M. Minogue, E. Thulin, D. M. Walsh, K. A. Dawson, S. Linse, *J. Am. Chem. Soc.* **2008**, *130*, 15437.